Spin-Current-Driven Permeability Variation for Time-Varying Magnetic Metamaterials

Toshiyuki Kodama, Nobuaki Kikuchi, Satoshi Okamoto, Seigo Ohno, and Satoshi Tomita

Phys. Rev. Applied **19**, 044080 — Published 26 April 2023

DOI: 10.1103/PhysRevApplied.19.044080

Spin-current Driven Permeability Variation for Time-varying Magnetic Metamaterials

Toshiyuki Kodama,[1,*] Nobuaki Kikuchi,[2] Satoshi Okamoto,[2,3] Seigo Ohno,[4] and Satoshi Tomita[1,4,†]

[1] *Institute for Excellence in Higher Education, Tohoku University, Sendai, 980-8576, Japan*

[2] *Institute of Multidisciplinary Research for Advanced Materials, Tohoku University, Sendai 980-8577, Japan*

[3] *Center for Science and Innovation in Spintronics, Tohoku University, Sendai 980-8577, Japan*

[4] *Department of Physics, Graduate School of Science, Tohoku University, Sendai 980-8578, Japan*

(Dated: March 28, 2023)

Abstract

We study permeability (μ) variation of a lithographically-prepared magnetic meta-atom consisting of Ta/Py/Pt trilayers by means of spin-torque ferromagnetic resonance (ST-FMR). With an injection of a direct current up to ± 20 mA together with an alternating current in GHz frequencies, the meta-atom under external magnetic fields shows significant changes in position and width of ST-FMR signals due to a massive spin-current injection. This leads to the spin-current driven μ variation, which is verified by analytical calculation based upon the experimentally obtained resonance field and Gilbert damping parameter. The present study paves a way to time-varying spintronic metamaterials with a high modulation frequency for realizing microwave sources toward the post-5th generation mobile communication system.

I. INTRODUCTION

Metamaterials are man-made structures, exhibiting exotic optical properties unavailable in natural materials. The most paradigmatic examples are metamaterials with negative refractive indices [1] and for invisible cloaks [2]. These are referred to as space-varying metamaterials because the refractive indices are modulated in space. Very recently, a paradigm for wave generation and manipulation has emerged using time-varying metamaterials, whose refractive indices are modulated in time [3]. The broken time-translation symmetry at the temporal boundary brings about the change in the refractive index while leaving the wavevector unchanged. As a consequence of the symmetry breaking, frequencies of electromagnetic waves have to change. Therefore, a long-term vision of time-varying metamaterials is achievement of the frequency leap by nonlinear up/down-conversion due to high modulation frequencies and large efficiencies.

Temporal modulation of the refractive index has been investigated so far using a variety of techniques; for example, commercially available electro-optical modulators, variable capacitance (varactor) diodes, photoexcited carrier generation in epsilon-near-zero materials [4, 5], plasma mirrors [6], photonic crystal nanocavities [7], structural-dispersion switching of waveguides [8], and microelectromechanical systems [9]. These techniques are based on

* Email address:tkodama@tohoku.ac.jp

† Email address:tomita@tohoku.ac.jp

electric permittivity (ε) modulation. Similarly, modulation of magnetic permeability (μ) is anticipated because μ is the counterpart of ε in the refractive index $n = \sqrt{\varepsilon}\sqrt{\mu}$. Nevertheless, μ modulation for time-varying metamaterial is lacking. The simultaneous modulation of both ε and μ is essential for realizing intriguing physical phenomena such as Fresnel drag effects for light without actual material motions [10].

In an electrical circuit analogue, ε modulation is assigned to a change in the capacitance, while μ modulation corresponds to an inductance variation. As inductance is relevant to turn numbers, length, and cross section of coils, time-varying μ intuitively seems to be a tough challenge. However, μ can be varied using magnetic materials. In particular, ferromagnetic materials have frequency dispersion of μ at a high frequency, i.e., in the vicinity of ferromagnetic resonance (FMR) frequencies in the GHz region. Moreover, a large magnetization, which originates from microscopic electron spins coupled in the ferromagnetic materials, causes a large variation in μ. Therefore, a significant μ modulation at GHz frequencies is achieved if the FMR conditions are modified somehow.

The FMR frequency is determined by effective magnetic fields and the gyromagnetic ratio γ, which is governed by the g-value [11–15]. Whereas γ is dependent on the magnetic materials and structures, the effective magnetic fields are controllable and changed externally. A key issue to be addressed is how the effective magnetic fields are changed in time. A possible way is a straightforward one with time-varying external magnetic fields applied by an electromagnet. However, the external magnetic fields is unlikely to be switched on and off at GHz frequencies. An alternative option is the utilization of magnetic fields due to a spintronic phenomenon, named spin-current, realized by the spin-Hall effect in heavy metals with large spin-orbit interaction, for example, tantalum (Ta) and platinum (Pt). The spin-current injection at GHz frequencies from Pt into ferromagnetic metal, like permalloy ($Fe_{80}Ni_{20}$; Py), results in a change in the magnetic fields for FMR, that is to say, spin-torque FMR (ST-FMR). In ST-FMR, the FMR frequency is varied by the spin-current amplitude. Moreover, the spin-current injection is likely to cause a change in the FMR lineshape, represented by the phenomenological Gilbert damping parameter α. The ST-FMR has intensively been investigated in the field of spintronics [16–21]. Contrastingly, μ variation due to an effective magnetic field change by the spin-current injection has yet to be explored.

Here, we experimentally study spin-current driven μ variation in lithographically-prepared magnetic microstructures consisting of Ta/Py/Pt trilayers as magnetic meta-atoms, which correspond to elementary components of magnetic metamaterials and determines primarily the metamaterials properties. An alternating (AC) current at GHz frequencies is injected to the microstructure under direct current (DC) magnetic fields to launch ST-FMR in the Py layer. In addition, a DC current is injected to the microstructure to modify the effective magnetic fields and the resonance condition. As the DC current increases, the ST-FMR signal shows a significant shift and narrowing due to massive spin-current injection. The shift and narrowing lead to the spin-current driven μ variation, which is verified by analytical calculation. These results represent a major step forward in the integration of metamaterials and spintronics. Furthermore, when magnetic meta-atoms are assembled into metamaterials and the DC current is replaced by yet another AC current at GHz frequencies, time-varying μ metamaterials can be realized. The present study thus paves a way to time-varying spintronic metamaterials with a high modulation frequency in realizing frequency translation of microwave for the post-5th generation (post-5G) mobile communication system.

II. THEORY OF PERMEABILITY VARIATION

In the following, letters in bold font styles denote vectors and normal style letters denote scalars. Consider magnetization $\boldsymbol{M}$ of a spherical ferromagnet with an effective magnetic field $\boldsymbol{H}_{\text{eff}}$ in the magnet. The equation of motion of $\boldsymbol{M}$ is expressed as

$$\frac{d\boldsymbol{M}}{dt} = -\gamma\mu_0 \boldsymbol{M} \times \boldsymbol{H}_{\text{eff}} + \frac{\alpha}{M_{\text{s}}}(\boldsymbol{M} \times \frac{d\boldsymbol{M}}{dt}), \tag{1}$$

where μ_0 is the permeability of vacuum, and M_s is the saturation magnetization [22]. Equation (1) is referred to as the Landau-Lifshitz-Gilbert equation. Suppose that an external DC magnetic field $\boldsymbol{H}_{\text{ext}}$, enough to saturate magnetization and obtain M_{s}, is applied to the sphere. Because there is no demagnetization fields in the sphere, $\boldsymbol{H}_{\text{eff}}$ is identical to $\boldsymbol{H}_{\text{ext}}$. The solution of Eq. (1) indicates that the magnetization precesses around the H_{ext}-field vector with a precession angular frequency, $\omega_0 = \gamma\mu_0 H_{\text{eff}} = \gamma\mu_0 H_{\text{ext}}$, called the Larmor frequency. The precession is damped in a period determined by α.

The magnetically saturated ferromagnet is then interacted with a weak AC (microwave) magnetic field $\boldsymbol{H}_{\text{AC}}$; $\boldsymbol{H}_{\text{eff}} = \boldsymbol{H}_{\text{ext}} + \boldsymbol{H}_{\text{AC}}$, where $|H_{\text{AC}}| << H_{\text{ext}}$. The $\boldsymbol{H}_{\text{AC}}$ has a frequency ω and a direction perpendicular to the H_{ext}-field axis, $\boldsymbol{H}_{\text{ext}} \perp \boldsymbol{H}_{\text{AC}}$. Such a field causes a forced precession at ω of the magnetization around the H_{ext}-field axis. When ω is swept in

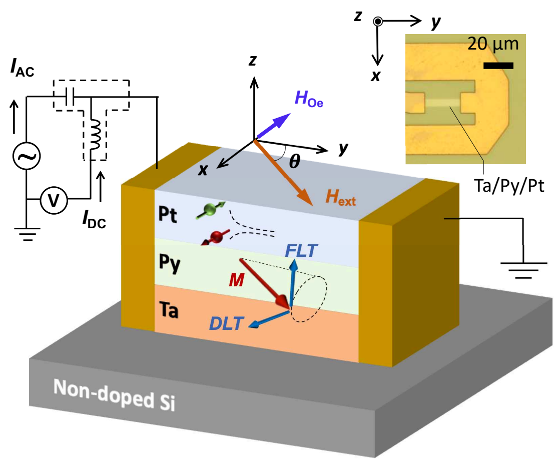

FIG. 1. Schematic illustration of magnetic meta-atom of Ta/Py/Pt trilayer with spin-torque ferromagnetic resonance measurement setup. Inset: photograph of lithographically-prepared magnetic meta-atom.

the GHz region, the energy of a microwave having $\omega = \omega_0$ is absorbed by the ferromagnet, giving rise to a resonance behavior referred to as FMR.

If the ferromagnetic material is not a sphere, $\boldsymbol{H}_{\mathrm{eff}}$ is affected by demagnetization fields $\boldsymbol{H}_{\mathrm{demag}}$ inside the material; $\boldsymbol{H}_{\mathrm{eff}} = \boldsymbol{H}_{\mathrm{ext}} + \boldsymbol{H}_{\mathrm{demag}} + \boldsymbol{H}_{\mathrm{AC}}$. The H_{demag} brings about a shift in the FMR angular frequency from ω_0 to ω_{FMR}. Figure 1 illustrates the structure of a magnetic meta-atom in the present study. The meta-atom consists of a ferromagnetic Py thin film sandwiched by heavy metal Ta and Pt thin films. For the ferromagnetic thin film, ω_{FMR} is described by the Kittel's equation [23] as

$$\omega_{\mathrm{FMR}} = \gamma\sqrt{\mu_0 H_{\mathrm{FMR}}(\mu_0 H_{\mathrm{FMR}} + \mu_0 M_{\mathrm{eff}})}, \tag{2}$$

where the effective magnetization $\mu_0 M_{\mathrm{eff}}$, which is similar to $\mu_0 M_{\mathrm{s}}$, corresponds to the demagnetization field. In the present experiments, $\mu_0 H_{\mathrm{ext}}$, not ω, is swept so that FMR is observed at $\mu_0 H_{\mathrm{ext}} = \mu_0 H_{\mathrm{FMR}}$.

Frequency dispersions of complex AC magnetic susceptibility $\chi(\omega)$ with magnetic losses is written using real $\chi'(\omega)$ and imaginary $\chi''(\omega)$ parts [24] as

$$\chi(\omega) = \chi'(\omega) - j\chi''(\omega), \tag{3}$$

where

$$\chi'(\omega) = \gamma M_{\mathrm{eff}} \frac{\omega_{\mathrm{FMR}}(\omega_{\mathrm{FMR}}^2 - \omega^2) + \omega_{\mathrm{FMR}}\omega^2\alpha^2}{[\omega_{\mathrm{FMR}}^2 - \omega^2(1+\alpha^2)]^2 + 4\omega_{\mathrm{FMR}}^2\omega^2\alpha^2}, \tag{4a}$$

$$\chi''(\omega) = \gamma M_{\mathrm{eff}} \frac{\alpha\omega[\omega_{\mathrm{FMR}}^2 - \omega^2(1+\alpha^2)]}{[\omega_{\mathrm{FMR}}^2 - \omega^2(1+\alpha^2)]^2 + 4\omega_{\mathrm{FMR}}^2\omega^2\alpha^2}, \tag{4b}$$

and $-j$ is the imaginary unit. To relate H and magnetic flux density B, we introduce complex relative magnetic permeability with magnetic losses, $\mu_{\mathrm{r}}(\omega)$, and have

$$B = \mu_0[1 + \chi(\omega)]H = \mu_0\mu_{\mathrm{r}}(\omega)H. \tag{5}$$

In this way, $\mu_{\mathrm{r}}(\omega)$ is written using real $\mu_{\mathrm{r}}'(\omega)$ and imaginary $\mu_{\mathrm{r}}''(\omega)$ parts as

$$\mu_{\mathrm{r}}(\omega) = 1 + \chi'(\omega) - j\chi''(\omega) = \mu_{\mathrm{r}}'(\omega) - j\mu_{\mathrm{r}}''(\omega). \tag{6}$$

In the present experiments in the following, we vary $\mu_{\mathrm{r}}(\omega)$ by injecting DC current into the meta-atom. The DC current modifies ω_{FMR} and α in Eq. (4). Using Eq. (2), ω_{FMR} is evaluated from $\mu_0 H_{\mathrm{FMR}}$, which is experimentally obtained from the ST-FMR measurements. Additionally, the ST-FMR measurements give values of α and $\mu_0 M_{\mathrm{eff}}$. Therefore complex $\mu_{\mathrm{r}}(\omega)$ is analytically calculated using $\mu_0 H_{\mathrm{FMR}}$, α and $\mu_0 M_{\mathrm{eff}}$ with Eqs. (4) and (6). More importantly, the present study demonstrates that the spin-current injection induced by the DC current modifies effective magnetic fields in the Py layer, leading to variations in $\mu_0 H_{\mathrm{FMR}}$ and α. From these variations, we evaluate how much $\mu_{\mathrm{r}}(\omega)$ is varied by the spin-current injection.

III. EXPERIMENTAL METHOD

Heavy metal layers of Ta and Pt, and a ferromagnetic metal layer of Py are deposited onto non-doped Si substrates at room temperature using magnetron sputtering with an argon (Ar) gas pressure of 6×10^{-1} Pa. A 3 nm thick Ta layer as a buffer layer is deposited on the substrates first, after which a Py layer of 2 nm and a Pt layer of 5 nm thickness are subsequently deposited. The Ta buffer layer is mainly for better adhesion and flatness of the Py layer on the substrate. The magnetization of the trilayer film is measured using a vibrating sample magnetometer (VSM). The trilayer film is then patterned into a rectangular shape of 5 µm width and 60 µm length using electron beam lithography (EBL) and Ar ion etching. The contact electrodes consisting of 5 nm thick Cr and 200 nm thick Au layers are prepared on the both sides of the rectangle using EBL and lift-off processes as shown in Fig. 1. The inset in Fig. 1 shows a photograph of the prepared magnetic meta-atom. The meta-atom length between the electrodes is 24 µm.

Figure 1 shows also a schematic illustration of the ST-FMR measurements [16]. An in-plane external DC magnetic field H_{ext} is applied using an electromagnet with a relative angle $\theta = 45°$ to the y-axis. An AC current I_{AC} at microwave frequencies in a range between 2 and 9 GHz is injected from a signal generator into the meta-atom along the y-axis. The signal generator's power of I_{AC} is -1 dBm. The I_{AC} induces an oscillating Oersted magnetic field $\boldsymbol{H}_{\mathrm{AC}}$ with the Ampere's law, primarily driving FMR of the Py magnetization. Moreover, the I_{AC} flowing in Pt and Ta layers generates vertical AC spin currents by the spin-Hall effect.

The direction of the spin-current is expressed by $\boldsymbol{J}_{\mathrm{spin}} \parallel \theta_{\mathrm{SH}}(\hat{\boldsymbol{\sigma}} \times \boldsymbol{J}_{\mathrm{charge}})$, where J_{spin} is the spin-current density, θ_{SH} is the spin-Hall angle, $\hat{\boldsymbol{\sigma}}$ is the Pauli spin matrix, and $\boldsymbol{J}_{\mathrm{charge}}$ is the charge current density. This equation indicates that the direction of $\boldsymbol{J}_{\mathrm{spin}}$ induced by $\boldsymbol{J}_{\mathrm{charge}}$ depends on θ_{SH}. Because θ_{SH} of Pt and Ta have the opposite signs [25], identical spin moments are injected to the Py layer from both the top Pt and bottom Ta layers. The $\boldsymbol{J}_{\mathrm{spin}}$ from the Pt layer is, however, much larger than that from the Ta layer because of large $\boldsymbol{J}_{\mathrm{charge}}$ in the Pt layer due to small electrical resistance compared to the Ta layer [26, 27]. Moreover, as the Ta layer deposited on the substrate is likely to be oxidized, the electrical resistance of the Ta layer is much larger, bringing about tiny $\boldsymbol{J}_{\mathrm{charge}}$ in the Ta layer. Thus the spin-current injection only from the Pt layer is considered in the following. The spin angular momentum injected from the Pt layer is transferred to the in-plane Py magnetization, exerting a field-like torque (FLT) that secondary drives magnetization precession and damping-like torque (DLT) that enhances or reduces magnetization relaxation. In this way, I_{AC} gives rise to an oscillating H_{AC}, FLT, and DLT, which drive ST-FMR in the Py layer.

Under the ST-FMR, the magnetization precession causes a resistance oscillating at the frequency of I_{AC} due to the anisotropic magnetoresistance (AMR) of Py. By mixing I_{AC} and the oscillating AMR, a time-independent longitudinal DC voltage V_{AMR} arises along the y-axis. We measure V_{AMR} as a function of $\mu_0 H_{\mathrm{ext}}$ using a bias tee [16, 28] to observe magnetization dynamics by ST-FMR and obtain $\mu_0 H_{\mathrm{FMR}}$ and α.

Variations in $\mu_0 H_{\mathrm{FMR}}$ and α is achieved by injecting a DC current I_{DC} together with I_{AC} into the meta-atom. The I_{DC} direction is parallel to that of I_{AC}. The I_{DC} leads to an time-independent Oersted DC field $\boldsymbol{H}_{\rm Oe}$ along $\pm x$-axis. Furthermore, $I_{\rm DC}$ generates a vertical DC spin-current in the Pt layer, giving rise to time-independent FLT and DLT on the Py magnetization as shown in Fig. 1. The FLT and DLT are regarded as internal magnetic fields $\boldsymbol{H}_{\rm spin}$ [29, 30]. The $\boldsymbol{H}_{\rm eff}$ acting on the magnetization can thus be given by $\boldsymbol{H}_{\rm eff} = \boldsymbol{H}_{\rm ext}+\boldsymbol{H}_{\rm demag}+\boldsymbol{H}_{\rm Oe}+\boldsymbol{H}_{\rm spin}$ as depicted in Fig. 1 when $\boldsymbol{H}_{\rm AC}$ and crystalline magnetic anisotropy are ignored. The $I_{\rm DC}$ injection causes variations in $H_{\rm Oe}$ and $H_{\rm spin}$, bringing about a change in $\mu_0 H_{\rm ext}$ for FMR, i.e., a shift in $\mu_0 H_{\rm FMR}$. Furthermore, the time-independent DLT influences α. When DLT has the same direction with the magnetization precession damping, the effective α is enhanced. Contrastingly, the effective α becomes small when the DLT direction is opposite to the damping. In the present experiments, $V_{\rm AMR}$ signals with various $I_{\rm AC}$ from 2 to 9 GHz and $I_{\rm DC}$ from -20 mA to $+20$ mA are measured as a function of $\mu_0 H_{\rm ext}$ in a range between $+150$ mT and -150 mT. All measurements are carried out at room temperature.

IV. RESULTS AND DISCUSSION

A. Spin-torque ferromagnetic resonance signals with alternating electric current

Figure 2(a) shows a typical $V_{\rm AMR}$ signal by ST-FMR measured with 6 GHz $I_{\rm AC}$ and zero $I_{\rm DC}$. The red open circles correspond to measurement results. The $V_{\rm AMR}$ signal in thin films is expressed as $V_{\rm AMR} = V_{\rm S} + V_{\rm A}$ [16, 17, 28], where

$$V_{\rm S} = S\frac{(\mu_0\Delta_{\rm FMR})^2}{(\mu_0 H_{\rm ext} - \mu_0 H_{\rm FMR})^2 + (\mu_0\Delta_{\rm FMR})^2}, \tag{7a}$$

$$V_{\rm A} = A\frac{\mu_0\Delta_{\rm FMR}(\mu_0 H_{\rm ext} - \mu_0 H_{\rm FMR})}{(\mu_0 H_{\rm ext} - \mu_0 H_{\rm FMR})^2 + (\mu_0\Delta_{\rm FMR})^2}. \tag{7b}$$

The $\mu_0\Delta_{\rm FMR}$ is the half width at half maximum of the FMR signal. The S in Eq. (7a) is a symmetric Lorentzian coefficient that is proportional to DLT, while A in Eq. (7b) is an anti-symmetric Lorentzian coefficient that is proportional to the oscillating $H_{\rm AC}$ and FLT. The measured $V_{\rm AMR}$ is fitted using Eqs. (7). The green and blue solid lines in Fig. 2(a) correspond to $V_{\rm S}$ and $V_{\rm A}$, respectively. The sum of $V_{\rm S}$ and $V_{\rm A}$ is represented by the black solid line, which reproduces well the experimental data. After the fitting, the $V_{\rm S}$ signal as well as $V_{\rm A}$ signal gives the resonance field $\mu_0 H_{\rm FMR} = 58.4$ mT and signal width $\mu_0\Delta_{\rm FMR} = 10.3$ mT.

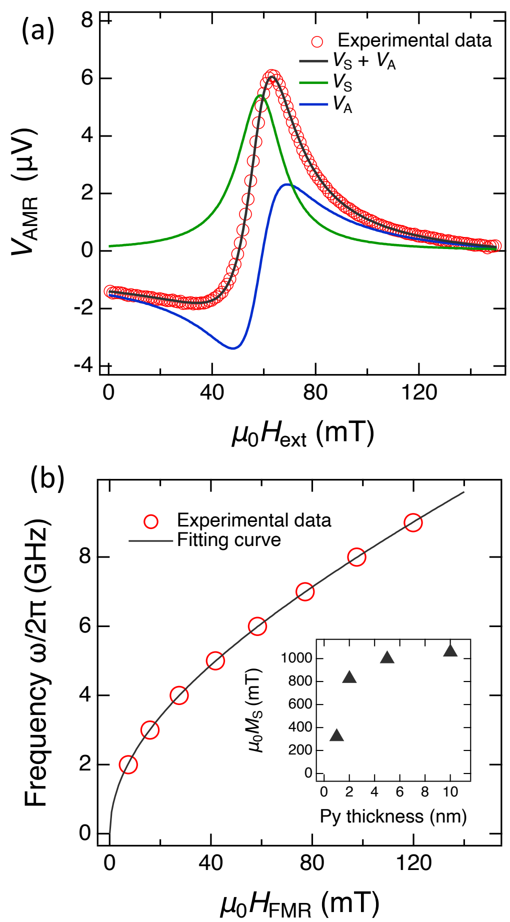

FIG. 2. (a) Measured spin-torque ferromagnetic resonance signal, V_{AMR}, as a function of external magnetic field, $\mu_0 H_{\mathrm{ext}}$, at 6 GHz without direct electric current (red circles). Green and blue solid lines represent fitting results with symmetric (V_{S}) and anti-symmetric coefficient (V_{A}), respectively. The black solid line corresponds to the sum of V_{S} and V_{A}. (b) Red circles: microwave frequency plotted as a function of resonance magnetic field, $\mu_0 H_{\mathrm{FMR}}$. Solid line: fitting curve by the Kittel equation [Eq. (2)]. Inset: trilayer's saturation magnetic flux density, $\mu_0 M_{\mathrm{s}}$, measured by VSM plotted as a function of Py thickness.

The frequency dependence of the V_{AMR} signals is acquired by keeping $I_{\mathrm{dc}} = 0$ but changing a I_{AC} frequency from 2 GHz to 9 GHz with intervals of 1 GHz. Figure 2(b) highlights the I_{AC} frequency versus $\mu_0 H_{\mathrm{FMR}}$ (red open circles). The black solid line in Fig. 2(b) corresponds to a fitting curve by the Kittel equation [Eq. (2)]. Given that the g-factor of the Py film is 2.1 [17], the fitting by Eq. (2) gives $\mu_0 M_{\mathrm{eff}} = 658$ mT. As in the inset of Fig. 2(b), VSM measurments show that the Ta/Py/Pt trilayer with 2 nm thick Py has saturation magnetic

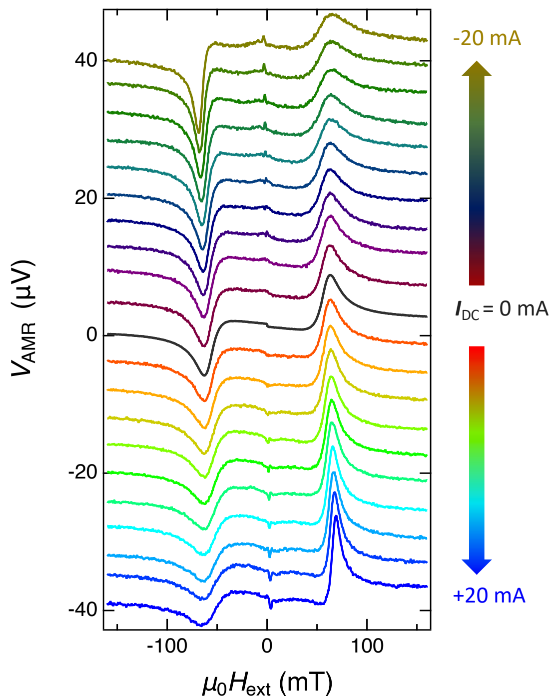

FIG. 3. Spin-torque ferromagnetic resonance signals with 6 GHz alternative electric currents measured at various direct electric currents, I_{DC} from -20 mA to $+20$ mA with intervals of 2 mA

flux density $\mu_0 M_{\mathrm{s}}$ of 805 mT. This value is similar to $\mu_0 M_{\mathrm{eff}}$ of 658 mT obtained from the ST-FMR measurements. The small difference between $\mu_0 M_{\mathrm{eff}}$ and $\mu_0 M_{\mathrm{s}}$ is probably caused by the Py thickness discrepancy in the two samples. This result indicates that the V_{AMR} signal originates from the uniform precession of electron spins in Py, referred to as the Kittel-mode FMR. Moreover, the inset of Fig. 2(b) shows trilayer film's $\mu_0 M_{\mathrm{s}}$ plotted as a function of Py thickness of 1, 2, 5, and 10 nm. Note here that $\mu_0 M_{\mathrm{s}}$ decrease significantly at the trilayer with 1 nm thick Py. The origin of the decrease is most likely the magnetic dead layer at the Py/Pt and Py/Ta interfaces [31].

B. Spin-torque ferromagnetic resonance signals with alternating and direct electric currents

Figure 3 shows V_{AMR} signals of ST-FMR with 6 GHz I_{AC} measured with various I_{DC} from -20 mA to $+20$ mA at intervals of 2 mA. A black solid line corresponds to a signal with $I_{\mathrm{DC}} = 0$ mA, a part of which is already shown in Fig. 2(a). A peak is seen at 70 mT in the V_{AMR} signal with $I_{\mathrm{DC}} = 0$ mA. As I_{DC} increases from 0 to +20 mA, the peak at 70 mT is getting narrower. Contrastingly, the peak becomes broader as I_{DC} decreases from 0 to -20 mA. When the direction of H_{ext} is reversed, the peaks change to dips because of the reversal in the relative angle between I_{AC} and H_{ext}. The variation of the dip lineshape at -70 mT is also inverted; the dip becomes broader as I_{DC} increases from -20 to +20 mA. The lineshape change depends on both the amplitude and direction of I_{DC}, indicating that the origin is the Joule heating as well as the spin-current injection and DC Oersted field.

The V_{AMR} signals at each I_{DC} between -20 to +20 mA are obtained by varying I_{AC} frequency from 2 to 9 GHz. The signals are analyzed using Eqs. (7) to evaluate $\mu_0 H_{\mathrm{FMR}}$ and $\mu_0 \Delta_{\mathrm{FMR}}$. In Fig. 4, $\mu_0 \Delta_{\mathrm{FMR}}$ evaluated at various I_{DC} is plotted as a function of I_{AC} frequency. Red open circles in Fig. 4 correspond to $\mu_0 \Delta_{\mathrm{FMR}}$ versus I_{AC} frequency at $I_{\mathrm{DC}} = 0$ mA. The frequency dependence of the signal linewidth gives the damping parameter α. The $\mu_0 \Delta_{\mathrm{FMR}}$ is expressed as

$$\mu_0 \Delta_{\mathrm{FMR}} = W + (\alpha/\gamma)\omega, \tag{8}$$

where W represents inhomogeneous linewidth broadening due to sample imperfections and is independent of the frequency of I_{AC}. A red solid line in Fig. 4 is a fitting curve of experimentally evaluated $\mu_0 \Delta_{\mathrm{FMR}}$ at $I_{\mathrm{DC}} = 0$ mA by Eq. (8). Equation (8) indicates that a slope of the fitting curve corresponds to α. The fitting at $I_{\mathrm{DC}} = 0$ mA gives $\alpha = 0.045 \pm 0.001$. Figure 4 highlights that, as I_{DC} increases from -20 to +20 mA, the fitting curve slope becomes smaller, indicating that a larger I_{DC} brings about a smaller α.

C. Direct electric current dependence of damping parameter and resonance field

In Fig. 5(a), the evaluated α (open circles) indicated from the left vertical axis is plotted as a function of I_{DC}. The α is 0.082 at $I_{\mathrm{DC}} = -20$ mA. As I_{DC} increases from -20 to +20 mA, α decreases monotonically and reaches the minimum value of 0.025 at $I_{\mathrm{DC}} = +20$ mA. This result clearly shows that α is controllable by the spin-current as reported previously in Refs. [16–18]. The variation in α is approximately 0.057, which is comparable to that reported in Ref. [19].

Open squares in Fig. 5(a) also shows a resonance field shift $\mu_0 H^{\mathrm{shift}}_{\mathrm{FMR}}(I_{\mathrm{DC}})$ by the I_{DC}

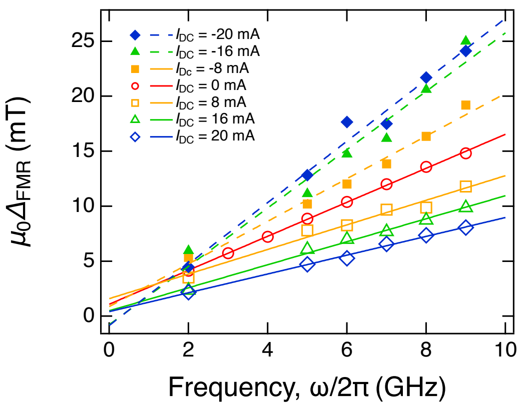

FIG. 4. Ferromagnetic resonance signal line width, $\mu_0\Delta_{\rm FMR}$, at various direct electric currents, $I_{\rm DC}$, from -20 mA to $+20$ mA as a function of $\omega/2\pi$. Solid and dashed lines are fitting curves.

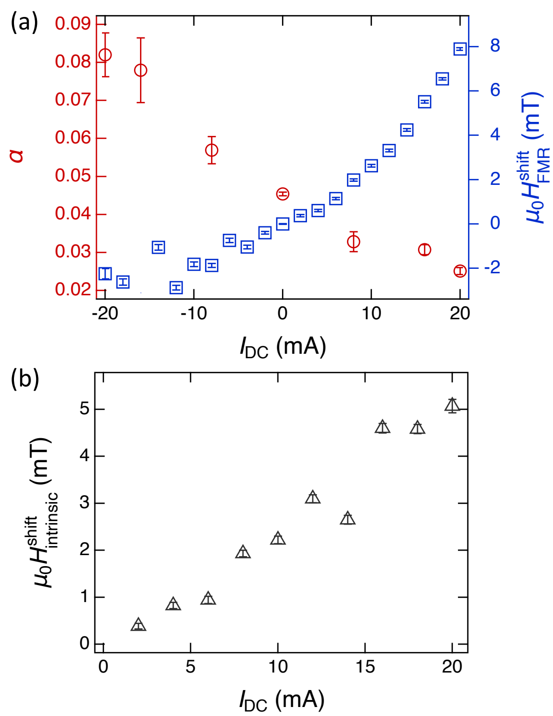

FIG. 5. (a) α (open circles, left axis) and $\mu_0 H^{\rm shift}_{\rm FMR}$ (open squares, right axis) are plotted as a function of $I_{\rm DC}$. (b) $\mu_0 H^{\rm shift}_{\rm intrinsic}$ (open triangles) is plotted as a function of $I_{\rm DC}$.

injection as indicated from the right axis. The $\mu_0 H^{\rm shift}_{\rm FMR}(I_{\rm DC})$ is defined as $\mu_0 H_{\rm FMR}(I_{\rm DC}) - \mu_0 H_{\rm FMR}(0)$, where $\mu_0 H_{\rm FMR}(I_{\rm DC})$ corresponds to $\mu_0 H_{\rm FMR}$ with non-zero specific $I_{\rm DC}$ and $\mu_0 H_{\rm FMR}(0)$ corresponds to $\mu_0 H_{\rm FMR}$ with zero $I_{\rm DC}$. A positive value of $\mu_0 H^{\rm shift}_{\rm FMR}$ represents a shift to a higher field. Figure 5(a) demonstrates that $\mu_0 H^{\rm shift}_{\rm FMR}(I_{\rm DC})$ is -2 mT at $I_{\rm DC} = -20$

mA and 8 mT at $I_{\mathrm{DC}} = 20$ mA.

As already mentioned, $\mu_0 H^{\mathrm{shift}}_{\mathrm{FMR}}(I_{\mathrm{DC}})$ is caused by the Joule heating, spin-current injection, and DC Oersted field. The enhanced fluctuations in magnetization by the Joule heating is a major factor in $\mu_0 H^{\mathrm{shift}}_{\mathrm{FMR}}$ [32]. The influence of the Joule heating is dependent on the electric current intensity, but independent of the current direction. On the other hand, the influence of the spin-current injection and Oersted field is a odd function of the I_{DC} direction. The Joule heating contribution can thus be removed by

$$\mu_0 H^{\mathrm{shift}}_{\mathrm{intrinsic}} = \frac{\mu_0 H^{\mathrm{shift}}_{\mathrm{FMR}}(I_{\mathrm{DC}}) - \mu_0 H^{\mathrm{shift}}_{\mathrm{FMR}}(-I_{\mathrm{DC}})}{2}, \tag{9}$$

and intrinsic resonance field shift, $\mu_0 H^{\mathrm{shift}}_{\mathrm{intrinsic}}$, due to the spin-current injection and Oersted field is obtained.

Figure 5(b) shows $\mu_0 H^{\mathrm{shift}}_{\mathrm{intrinsic}}$ as a function of I_{DC}. The $\mu_0 H^{\mathrm{shift}}_{\mathrm{intrinsic}}$ increases linearly with an increase in I_{DC}. The slope is approximately 0.27 mT/mA. Using current density in the sample, this value is transfromed to 6.25×10^{-12} mT/(A/m^2), which is similar to 4.24×10^{-12} mT/(A/m^2) in Ref. [17]. However, the amount of the shift obtained in this study is much larger than that in the previous studies [17, 29, 30, 33]. Thanks to the well-insulated non-doped Si substrate with better thermal conductivity [34, 35], we can inject massive I_{DC} up to 20 mA, which causes the large shift variation of approximately 5 mT while the previously reported one is less than 0.7 mT.

D. Evaluation of permeability variation

In order to evaluate $\mu'_{\mathrm{r}}(\omega)$ and $\mu''_{\mathrm{r}}(\omega)$ at a specific I_{DC} value from Eq. (6), $\chi'(\omega)$ and $\chi''(\omega)$ should be calculated from Eq. (4) with ω_{FMR}, α, and M_{eff} experimentally obtained at the I_{DC} value. First, $\mu'_{\mathrm{r}}(\omega)$ and $\mu''_{\mathrm{r}}(\omega)$ of the meta-atom under DC magnetic field of 58.4 mT at $I_{\mathrm{DC}} = 0$ mA are calculated from Eqs. (4) and (6). We use $\omega_{\mathrm{FMR}}/2\pi = 6$ GHz, $\mu_0 M_{\mathrm{eff}} = 658$ mT obtained in Fig. 2, and $\alpha = 0.045$ obtained in Fig. 4. Then, spin-current injection by non-zero I_{DC} values causes variations of $\omega_{\mathrm{FMR}}/2\pi$ from 6 GHz at $I_{\mathrm{DC}} = 0$ mA as shown in Fig. 5(b) through variation in $\mu_0 H_{\mathrm{FMR}}$. The spin-current injection also leads to variations of α from 0.045 at $I_{\mathrm{DC}} = 0$ mA as shown in Fig. 5(a). The I_{DC} dependence of α in Fig. 5(a) is thus fitted by a linear function. Similarly, another linear function is acquired by a fit of I_{DC} dependence of $\mu_0 H^{\mathrm{shift}}_{\mathrm{intrinsic}}$ in Fig. 5(b). These fitting functions give α and $\mu_0 H_{\mathrm{FMR}}$ at

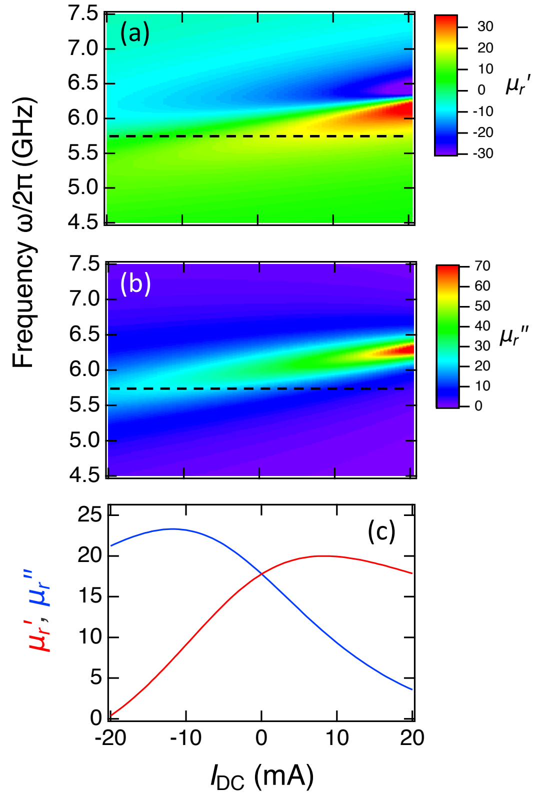

FIG. 6. 2D plot of (a) μ_{r}' and (b) μ_{r}'' evaluated using experimentally obtained α and $\mu_0 H_{\mathrm{FMR}}$ of meta-atom under DC magnetic field of 58.4 mT as a function of $\omega/2\pi$ and I_{DC}. Black dashed lines indicate $\omega/2\pi$ = 5.74 GHz. (c) I_{DC} versus μ_{r}' (red solid line) and μ_{r}'' (blue dashed line) at 5.74 GHz indicated by black dashed lines in (a) and (b).

a specific I_{DC} value. Given that I_{DC} do not influence the Kittel formula of Eq. (2), $\mu_0 M_{\mathrm{eff}}$ = 658 mT, and $\gamma = 1.87 \times 10^{-11}$ Hz/T, $\mu_0 H_{\mathrm{FMR}}$ is converted to ω_{FMR} at each I_{DC} from Eq. (2). Finally, from Eqs. (4) and (6) using ω_{FMR}, α, and M_{eff}, $\mu_{\mathrm{r}}'(\omega)$ and $\mu_{\mathrm{r}}''(\omega)$ at each I_{DC} are analytically obtained.

Figures 6(a) and 6(b) respectively show 2D plots of μ_{r}' and μ_{r}'' of the meta-atom under DC magnetic field of 58.4 mT as a function of $\omega/2\pi$ and I_{DC}. In Fig. 6(a), red color in the plot is assigned to a positive value of μ_{r}', whereas blue is assigned to a negative value. In Fig. 6(b), μ_{r}'' varies from 0 (blue) to 70 (red). The vertical cross-sections of the 2D plots correspond to frequency dispersions of μ_{r}' and μ_{r}'' at a specific I_{DC} value. Figures 6(a) and 6(b) shows that a larger I_{DC} brings about a larger variation in μ_{r}' and μ_{r}''.

Figure 6(c) highlights I_{DC} versus μ_{r}' (red line) and μ_{r}'' (blue line) at 5.74 GHz, which is indicated by black dashed lines in Figs 6(a) and 6(b). In Fig. 6(c), μ_r' at 5.74 GHz shows a small value of 0.4 at I_{DC} = -20 mA, increases with I_{DC}, and exhibits a maximum value of 20.0 at I_{DC} = +8.5 mA. After the maximum value, μ_r' slightly decreases to 17.8 at I_{DC} = +20 mA. Contrastingly, μ_r'' at 5.74 GHz has a large value of 21.2 at I_{DC} = -20 mA. The μ_r'' shows a maximum value of 23.3 at I_{DC} = -12 mA, and decreases down to 3.6 at I_{DC} = +20 mA. The large variation in μ_r' and μ_r'' is primarily caused by the massive I_{DC} up to ± 20 mA.

Let us consider a spin-current driven frequency up-conversion of a microwave having 5.74 GHz by the time-varying magnetic meta-atom under DC magnetic field of 58.4 mT. An AC current at 5.74 GHz as a carrier wave flows through the meta-atom. Instead of the DC current, another AC current having an amplitude of 20 mA and a frequency that is lower than 5.74 GHz, for example, 1 GHz, is also injected to generate a magnetic field by the spin-current injection for modulation. If a simple phase modulation is supposed, the 5.74 GHz carrier microwave in the meta-atom "feels" time-varying μ_r' between 0.4 and 17.8 at a modulation frequency of 1 GHz, leading to a creation of a modulated microwave having 6.74 GHz. The up-converted 6.74 GHz microwave can be radiated from an antenna connected to the meta-atom. Furthermore, in addition to the phase modulation, amplitude modulation due to time-varying μ_r'' between 3.6 and 21.2 is likely and may realize a large modulation amplitude. Because the variation in μ_r' and μ_r'' is not a linear function of I_{DC} as in Fig. 6(c), a modulation frequency at 1GHz gives rise to μ_r' and μ_r'' variation at a much higher frequency. Last but at least, it is worth mentioning that natural antiferromagnets, for example, NiO [36], and artificial antiferromagnetic structures, for example, Co/Ru multilayers, are possible candidates for permeability modulation at much higher frequencies in millimeter wave and THz light regions.

V. CONCLUSION

We experimentally demonstrate spin-torque ferromagnetic resonance (ST-FMR) of a lithographically-prepared magnetic meta-atom consisting of Ta/Py/Pt trilayer thin films on non-doped Si substrates. The ST-FMR in the Py layer is performed by injecting a large direct electric current up to ± 20 mA together with an alternating electric current at GHz frequencies to the meta-atom under DC magnetic fields. Thanks to the well-insulated substrates with a better thermal conductivity, the massive spin-current injection gives rise to significant changes in damping parameter α, and FMR field $\mu_0 H_{\rm FMR}$; α becomes approximately 1/3 and the maximum amount of shift of $\mu_0 H_{\rm FMR}$ is 5 mT. From analytical calculation based on the experimentally obtained α and $\mu_0 H_{\rm FMR}$, we verify large variations in the real part of permeability from 0.4 to 17.8 and the imaginary part of permeability from 3.6 to 21.2 at 5.74 GHz for the meta-atom under DC magnetic field of 58.4 mT. The spin-current driven magnetic permeability variation can be realized by combining a magnetic Py layer with heavy-metal Pt and Ta layers, thus highlighting a major step forward in the integration of metamaterials with spintronics. The present study opens a door for an avenue of time-varying spintronic metamaterials with a GHz modulation frequency.

ACKNOWLEDGMENT

The authors acknowledge M. Hatayama, K. Sawada, T. Nakanishi, Y. Kanamori for their valuable contributions in this work. N. K., S. O., and S. T. also thank Network Joint Research Center for Materials and Devices (NJRC). This work is financially supported by JST- CREST (JPMJCR2102).

[1] R. A. Shelby, D. R. Smith, and S. Schultz, Experimental verification of a negative index of refraction, Science **292**, 77 (2001).

[2] D. Schurig, J. J. Mock, B. J. Justice, S. A. Cummer, J. B. Pendry, A. F. Starr, and D. R. Smith, Metamaterial electromagnetic cloak at microwave frequencies, Science **314**, 977 (2006).

[3] E. Galiffi, R. Tirole, S. Yin, H. Li, S. Vezzoli, P. A. Huidobro, M. G. Silveirinha, R. Sapienza, A. Alú, and J. B. Pendry, Photonics of time-varying media, Advanced Photonics **4**, 0140022 (2022).

[4] Y. Zhou, M. Z. Alam, M. Karimi, J. Upham, O. Reshef, C. Liu, A. E. Willner, and R. W. Boyd, Broadband frequency translation through time refraction in an epsilon-near-zero material, Nat. Commun. **11**, 1 (2020).

[5] M. Z. Alam, S. A. Schulz, J. Upham, I. De Leon, and R. W. Boyd, Large optical nonlinearity of nanoantennas coupled to an epsilon-near-zero material, Nat. Photonics **12**, 79 (2018).

[6] R. L. Savage, C. Joshi, and W. B. Mori, Frequency upconversion of electromagnetic radiation upon transmission into an ionization front, Phys. Rev. Lett. **68**, 946 (1992).

[7] T. Tanabe, M. Notomi, H. Taniyama, and E. Kuramochi, Dynamic Release of Trapped Light from an Ultrahigh-Q Nanocavity via Adiabatic Frequency Tuning, Phys. Rev. Lett. **102**, 043907 (2009).

[8] F. Miyamaru, C. Mizuo, T. Nakanishi, Y. Nakata, K. Hasebe, S. Nagase, Y. Matsubara, Y. Goto, J. Pérez-Urquizo, J. Madéo, and K. M. Dani, Ultrafast Frequency-Shift Dynamics at Temporal Boundary Induced by Structural-Dispersion Switching of Waveguides, Phys. Rev. Lett. **127**, 053902 (2021).

[9] Y. Huang, K. Nakamura, Y. Takida, H. Minamide, K. Hane, and Y. Kanamori, Actively tunable THz filter based on an electromagnetically induced transparency analog hybridized with a MEMS metamaterial, Sci. Rep. **10**, 20807 (2020).

[10] P. A. Huidobro, E. Galiffi, S. Guenneau, R. V. Craster, and J. B. Pendry, Fresnel drag in space-time-modulated metamaterials, Proc. Natl. Acad. Sci. USA **116**, 24943 (2019).

[11] S. Tomita, K. Sawada, A. Porokhnyuk, and T. Ueda, Direct Observation of Magnetochiral Effects through a Single Metamolecule in Microwave Regions, Phys. Rev. Lett. **113**, 235501 (2014).

[12] T. Kodama, S. Tomita, T. Kato, D. Oshima, S. Iwata, S. Okamoto, N. Kikuchi, O. Kitakami, N. Hosoito, and H. Yanagi, Ferromagnetic Resonance of a Single Magnetochiral Metamolecule of Permalloy, Phys. Rev. Appl. **6**, 024016 (2016).

[13] S. Tomita, H. Kurosawa, T. Ueda, and K. Sawada, Metamaterials with magnetism and chirality, J. Phys. D: Appl. Phys. **51**, 083001 (2018).

[14] T. Kodama, Y. Kusanagi, S. Okamoto, N. Kikuchi, O. Kitakami, S. Tomita, N. Hosoito, and H. Yanagi, Microwave Spectroscopy of a Single Permalloy Chiral Metamolecule on a Coplanar Waveguide, Phys. Rev. Appl. **9**, 054025 (2018).

[15] S. Tomita, N. Kikuchi, and S. Okamoto, Co-planar waveguide ferromagnetic resonance spectroscopy of cobalt/platinum superlattice metamaterials, Jpn. J. Appl. Phys. **62**, SB1010 (2023).

[16] L. Liu, T. Moriyama, D. C. Ralph, and R. A. Buhrman, Spin-Torque Ferromagnetic Resonance Induced by the Spin Hall Effect, Phys. Rev. Lett. **106**, 036601 (2011).

[17] T. Nan, S. Emori, C. T. Boone, X. Wang, T. M. Oxholm, J. G. Jones, B. M. Howe, G. J. Brown, and N. X. Sun, Comparison of spin-orbit torques and spin pumping across NiFe/Pt and NiFe/Cu/Pt interfaces, Phys. Rev. B Condens. Matter **91**, 214416 (2015).

[18] K. Ando, S. Takahashi, K. Harii, K. Sasage, J. Ieda, S. Maekawa, and E. Saitoh, Electric Manipulation of Spin Relaxation Using the Spin Hall Effect, Phys. Rev. Lett. **101**, 036601 (2008).

[19] S. Kasai, K. Kondou, H. Sukegawa, S. Mitani, K. Tsukagoshi, and Y. Otani, Modulation of effective damping constant using spin Hall effect , Appl. Phys. Lett. **104**, 092408 (2014).

[20] L. Chen, X. Zhan, K. Zhou, W. Wang, L. Liang, Z. Gao, Y.W. Du, and R.H. Liu, Spin-Orbit-Torque Efficiency and Current-Driven Coherent Magnetic Dynamics in a Pt/Ni/Py Trilayer-Based Spin Hall Nano-Oscillator, Phys. Rev. Applied, **17**, 064041 (2022).

[21] M. Haidar, A. A. Awad, M. Dvornik, R. Khymyn, A. Houshang, and J. Åkerman, A single layer spin-orbit torque nano-oscillator, Nat. Commun. **10**, 2362 (2019).

[22] T. L. Gilbert, A phenomenological theory of damping in ferromagnetic materials, IEEE Trans. Magn. **40**, 3443 (2004).

[23] C. Kittel, On the Theory of Ferromagnetic Resonance Absorption, Phys. Rev. **73**, 155 (1948).

[24] D. Pozar, *Microwave Engineering*, 4th Edition (Wiley, New York, 2011).

[25] M. Morota, Y. Niimi, K. Ohnishi, D. H. Wei, T. Tanaka, H. Kontani, T. Kimura, and Y. Otani, Indication of intrinsic spin Hall effect in $4d$ and $5d$ transition metals, Phys. Rev. B Condens. Matter **83**, 174405 (2011).

[26] M.-H. Nguyen, D. C. Ralph, and R. A. Buhrman, Spin Torque Study of the Spin Hall Conductivity and Spin Diffusion Length in Platinum Thin Films with Varying Resistivity, Phys. Rev. Lett. **116**, 126601 (2016).

[27] S. M. Rossnagel, Characteristics of ultrathin Ta and TaN films, J. Vac. Sci. Technol. B **20**, 2328 (2002).

[28] Y. Wang, R. Ramaswamy, and H. Yang, FMR-related phenomena in spintronic devices, J. Phys. D Appl. Phys. **51**, 273002 (2018).

[29] M. Kawaguchi, T. Moriyama, T. Koyama, D. Chiba, and T. Ono, Layer thickness dependence of current induced effective fields in ferromagnetic multilayers, J. Appl. Phys. **117**, 17C730 (2015).

[30] R. W. Greening, D. A. Smith, Y. Lim, Z. Jiang, J. Barber, S. Dail, J. J. Heremans, and S. Emori, Current-induced spin–orbit field in permalloy interfaced with ultrathin Ti and Cu, Appl. Phys. Lett. **116**, 052402 (2020).

[31] S. Hirayama, S. Kasai, and S. Mitani, Interface perpendicular magnetic anisotropy in ultrathin Ta/NiFe/Pt layered structures, Jpn. J. Appl. Phys. **57**, 013001 (2017).

[32] V. E. Demidov, S. Urazhdin, E. R. J. Edwards, M. D. Stiles, R. D. McMichael, and S. O. Demokritov, Control of Magnetic Fluctuations by Spin Current, Phys. Rev. Lett. **107**, 107204 (2011).

[33] C. Kim, D. Kim, B. S. Chun, K.-W. Moon, and C. Hwang, Evaluation Method for Fieldlike-Torque Efficiency by Modulation of the Resonance Field, Phys. Rev. Applied **9**, 054035 (2018).

[34] G. A. Slack, Thermal Conductivity of Pure and Impure Silicon, Silicon Carbide, and Diamond, J. Appl. Phys. **35**, 3460 (1964).

[35] T. Yamane, N. Nagai, S.-I. Katayama, and M. Todoki, Measurement of Thermal Conductivity of Silicon Dioxide Thin Films Using a 3ω Method, J. Appl. Phys. **91**, 9772 (2002).

[36] T. Moriyama, K. Hayashi, K. Yamada, M. Shima, Y. Ohya, T. Ono, Tailoring THz Antiferromagnetic Resonance of NiO by Cation Substitution, Phys. Rev. Mater. **4**, 074402 (2020).